A PSO Solution for Improved Voltage Stability of a Hybrid AC-DC Microgrid

M. Akbari, M.A. Golkar, and S.M.M. Tafreshi
Electrical and Computer Engineering Department
K.N. Toosi University of Technology
Tehran, Iran
mohsenakbari@ieee.org , golkar@eetd.kntu.ac.ir , tafreshi@eetd.kntu.ac.ir

***Abstract*—The stability of dc and ac bus voltage is of the most important issues in all microgrids including ac, dc or ac/dc hybrid microgrids. In this paper, a hybrid ac/dc microgrid is proposed to reduce processes of multiple reverse conversions in an ac or dc microgrid and to facilitate the connection of various renewable ac and dc sources and loads to power system. Also, all control schemes used among all converters will be developed in order to improve the voltage stability of hybrid microgrid. To give robustness to improved dynamic voltage stability of the microgrid, a voltage stabilizer is proposed and applied to the doubly fed induction generator (DFIG) installed in ac part. Furthermore, a particle swarm optimization (PSO) solution is proposed to optimize the various control gains among various converters in order to quickly restore and stabilize the voltage of both ac and dc parts under the different disturbances. The achieved results verify the controllers robustness and optimization algorithm efficiency.**

Keywords- controller; hybrid ac/dc microgrid; PSO algorithm; voltage stability

I. INTRODUCTION

Nowadays, it is preferred to integrate renewable energies in the microgrid in order to reduce the CO_2 emission and the fossil fuel consumption. The benefits of distributed energy resources are seen to be higher reliability of service, better quality of power supply, and greater efficiency of energy use by utilizing the available waste heat from power generation systems. In addition, the ability to use renewable energy with little or no pollution is becoming increasingly attractive for environmental protection considerations and attracts increasingly important interests. Furthermore, distributed generation can benefit the electric utility by reducing congestion on the grid, reducing the need for new generation and transmission capacity, and offering ancillary services [1].

The ac microgrids [2]–[6] have been proposed to facilitate the connection of renewable energy sources to conventional ac systems. However, dc power from some distributed generators, such as photovoltaic (PV) panels or fuel cells, has to be converted into ac using dc/dc boosters and dc/ac inverters in order to connect to an ac grid. In an ac grid, embedded ac/dc and dc/dc converters are required for various home and office facilities to supply different dc voltages [7].

Recently, dc microgrids are resurging due to the development and deployment of renewable dc power sources and their inherent advantage for dc loads in commercial, industrial and residential applications [8]–[11]. However, ac sources have to be converted into dc before connected to a dc grid and dc/ac inverters are required for conventional ac loads.

Multiple reverse conversions required in individual ac or dc grids may add additional loss to the system operation and will make the current home and office appliances more complicated [7].

The smart grid concept is currently prevailing in the electric power industry. The objective of constructing a smart grid is to provide reliable, high quality electric power to digital societies in an environmentally, friendly and sustainable way. One of most important futures of a smart grid is the advanced structure which can facilitate the connections of various ac and dc generation systems, energy storage options, and various ac and dc loads with the optimal asset utilization and operation efficiency [7]. To achieve those goals, power electronics technology and control schemes play the most important roles to interface different sources and loads to a smart grid.

In [7], [12]-[14] hybrid ac/dc microgrids are proposed to reduce processes of multiple reverse conversions in an individual ac or dc microgrid and to facilitate the connection of various renewable ac and dc sources and loads to power system. So in this paper, a hybrid ac/dc microgrid is proposed and studied.

Since in all the microgrids, the stability of dc and ac bus voltage is of the most important issues, so in this study, voltage stability control of a hybrid microgrid is studied. Also, a voltage stabilizer is proposed to improve the dynamic voltage stability of proposed hybrid microgrid. It was applied to a doubly fed induction generator (DFIG) installed in ac part.

Furthermore, in this paper a particle swarm optimization (PSO) solution is proposed to optimize the various control gains among various converters in order to maintain the stable voltage of both ac and dc parts under disconnection from (islanding) and connection to the utility grid and fault permanently occurrence. PSO is a novel population based meta-heuristic, which utilizes the swarm intelligence generated by the cooperation and competition between the particles in a swarm and has emerged as the useful tool for engineering optimization. Unlike the other heuristic techniques, it has a flexible and well-balanced mechanism to

978-1-4673-0315-6/11/$26.00©2011 IEEE

enhance the global and local exploration abilities. This algorithm has also been found to be robust in solving problems featuring non-linearity, non-differentiability and high-dimensionality [15].

II. System Configuration and Resources Modeling

A. Proposed Hybrid Microgrid Configuration

A hybrid microgrid as shown in Fig. 1 is proposed and modeled in MATLAB/Simulink.

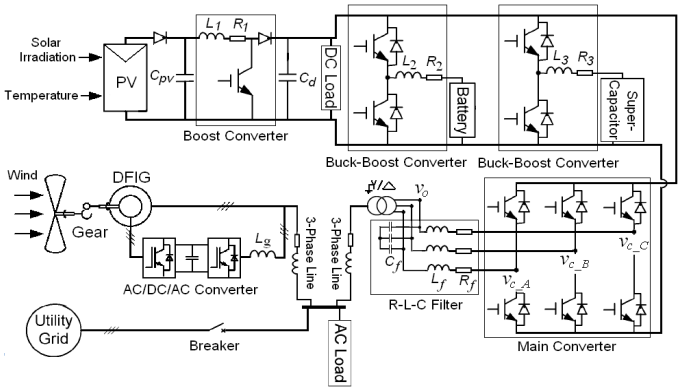

Figure 1. A compact representation of the proposed hybrid microgrid

PV array is connected to dc bus through a dc/dc boost converter to simulate dc sources. A capacitor C_{pv} is used to suppress high frequency ripples of the PV output voltage [7].

Also, a wind turbine (WT) with DFIG is connected to an ac bus to simulate ac sources. In addition, a battery and a super-capacitor as the energy storages are separately connected to dc bus through bidirectional (buck-boost) dc/dc converters. dc and ac loads are also connected to dc and ac buses, respectively. The dc load was considered as a pure resistive load, but the connected ac load was included constant-impedance (resistance-inductance), constant-capacitance, and constant-power (induction motor) loads. The rated voltages for dc and ac parts are 400 V and 400 V rms, respectively. A 3-phase bidirectional dc/ac main converter with R-L-C filter connects the dc part to the ac part through an isolation transformer. Furthermore, Two similar ac lines are considered with impedance 0.0024+j*0.000212 Ω.

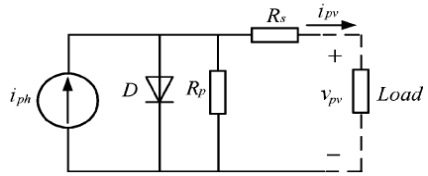

Figure 2. Equivalent circuit of a solar panel

B. Modeling of Energy Resources

1) PV Array

Fig. 2 shows an equivalent circuit of a PV panel modeled by a controlled current source. i_{pv} and v_{pv} are terminal current and voltage of the PV panel, respectively. The current output of the PV panel was modeled by formula shown in [7]. Also, 40 kW PV panel parameters, used in study, were extracted from [7].

2) Battery and Super-Capacitor Storages

Although renewable resources are attractive, they are not always dependable in the absence of energy storage devices. The utilization of energy storage units in power systems can be classified into two categories. One is in response to fast transients and the other is related to steady-state energy exchanging. Super-capacitors are good candidates for the former application and batteries are suitable for the latter one. Currently, the mixed use of fast and slow energy storage units is gaining popularity for interconnection of renewable generation [16].

In this study, a 65 Ah, 200 V nickel-metal-hydride (NiMH) battery was used together with a super-capacitor storage. The battery was modeled using a controlled nonlinear voltage source in series with a constant resistance as shown in [17].

One of the important parameters to represent state of a battery is state-of-charge (SOC) defined as [17]:

$$SOC\,\% = 100\left(1 - \frac{it}{Q}\right) \tag{1}$$

where it is the extracted capacity and Q is the maximum capacity of battery storage. The battery SOC is between 0%, for an empty battery, and 100%, for a fully charged battery.

Also, in modeling of the present 500 F super-capacitor storage, it was assumed that it is an ideal capacitance, i.e. its resistance was exactly considered to zero.

3) Wind Turbine Generator

In this study, DFIG was considered as a wound rotor induction machine, which needs to excite at both the stator and rotor terminals. Modeling of DFIG is well shown in SimPowerSystem Library of MatLab software. The 50 kW DFIG parameters, used in this study, were extracted from [7].

III. Controllers

The hybrid microgrid can operate in two modes: grid-connected mode and islanded mode. In this study system, when ac part of microgrid is directly connected to the utility grid, the magnitude of dc part voltage can be regulated by the parallel inverters and energy resources located in dc part. And the magnitude and frequency of ac part voltage are the same with the utility grid. However, when the microgrid works in islanded operation mode, dc part voltage must be regulated by only microsources and storages located in dc part. And the magnitude and frequency of ac part are controlled by parallel inverters. The controllers used for both operating modes are described in the following sub-sections.

A. Grid-Connected Mode

1) Boost Converter Controller

When the hybrid microgrid operates in this mode, the control objective of the boost converter is to track the

maximum power point (MPPT) of the PV panel. To achieve this objective, P&O method proposed in [18]-[19] was used.

2) Coordinated Control of Battery, Super-Capacitor and Main Converter

Battery has high energy density whereas it has relatively slow charging and discharging speed. On the other hand, super-capacitor has high power density and fast response. The mixed use of these energy storage units can make them complimentary to each other. Based on the above characteristics of battery and super-capacitor, a hybrid control scheme was designed as shown in Fig. 3.

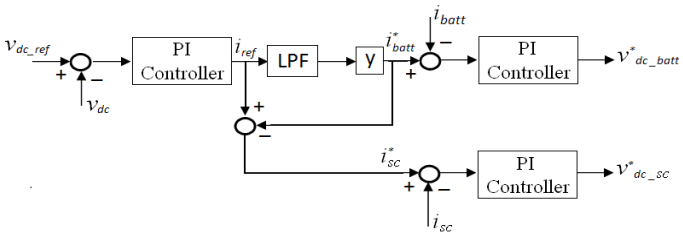

Fig. 3. Coordinated control scheme of the battery and super-capacitor storages

In this scheme, the dc part voltage is coordinately controlled by battery and super-capacitor storages. First, the measured dc part voltage v_{dc} is compared with its reference $v_{dc\text{-}ref}$ and the difference is sent to a proportional-integration (PI) controller to get the current reference i_{ref}. Then i_{ref} is split into two parts. One is the battery current reference i^*_{batt} which is obtained by applying a low-pass filter (LPF) with a cut-off frequency 25 Hz and a coefficient y (equal to 0.8 in this study) to i_{ref}. The other one i^*_{sc} is the difference between i_{ref} and i^*_{batt}. By this means, the high frequency part of the dc part disturbance and somehow low frequency part will be mitigated by super-capacitor and the remained low frequency part of the disturbance is smoothed by battery. The current references i^*_{sc} and i^*_{batt} will be used in the constant current control of the buck-boost converters shown in Fig. 1.

But, the battery has limits on SOC value. If SOC value is reached to its bounds, then the battery will be out and main converter will do the battery task to smooth remained low frequency part of the dc part disturbance. In other words, i^*_{batt} will be displaced by i^*_{fd}. The upper and lower bounds of battery SOC are considered 90% and 60%, respectively. Also, the main converter was designed to provide a pre-defined reactive power. The proposed control scheme and detailed schematic of main converter are shown in Figs. 4 and 5, respectively.

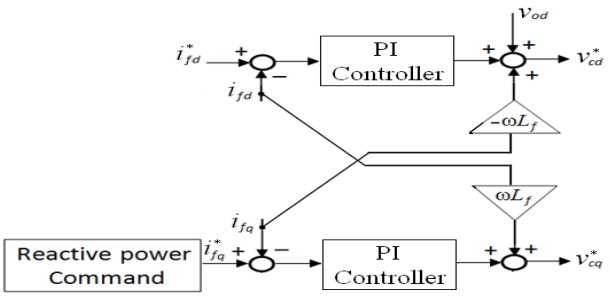

Figure 4. Control scheme of main converter in grid-connected mode

1) DFIG Controller

DFIG has several controllers that are: rotor-side converter controller, grid-side converter controller, pitch controller and torque controller. The objectives of the rotor-side converter

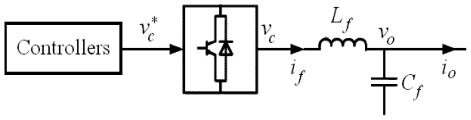

Figure 5. Detailed schematic of the main converter

are to manage the stator-side active and reactive powers. The DTC scheme proposed in [7] was selected as the control method for the rotor-side converter in this study. The rotor rotational speed was obtained through the MPPT algorithm, based on algorithm proposed in [20], to track the MPPT of WT.

The grid-side converter was designed to regulate the voltage of its own dc-link capacitor. In addition, this model allows using grid-side converter to generate or absorb reactive power. This control system is illustrated in Fig. 6. The voltage of the dc-link is controlled by i_{dg}, while the reactive power is controlled by i_{qg}.

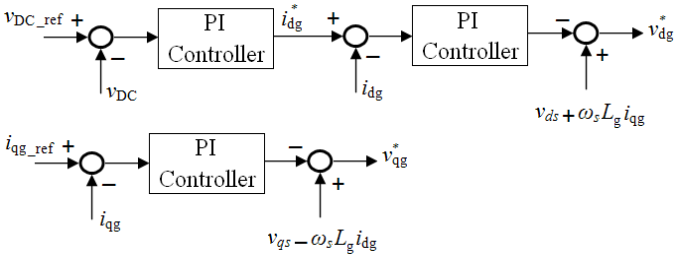

Figure 6. Grid-side converter control block diagram

Also, pitch control scheme proposed in [21] was used for DFIG. The controller enforces the rotor speed related to MPPT as a reference speed. Also, pitch compensation was done in this scheme. When the available wind power is less than rated, the blades are fixed to maximize the mechanical power, and when the available wind power is above the equipment rating, the blades are pitched to reduce P_{mech} delivered to the shaft down to the mechanical power 1.0 pu.

Furthermore, the torque control scheme proposed in [21] was accomplished by using rotor speed reference. The torque controller output was used in rotor-side converter controller to calculate the d-axis current reference.

Also in this study, a voltage stabilizer applied in DFIG was proposed and designed to improve the voltage of ac grid as shown in Fig. 7. High frequency part of positive sequence voltage of ac grid is compensated by q-axis current of grid-side converter and its low frequency part is compensated by d-axis and q-axis currents of rotor-side converter. The cut-off frequency of LPF and high-pass filter (HPF) was selected to 10 kHz.

B. *Islanded Mode*

In islanded mode, all the controllers used in grid-connected mode were again applied, except some modifications which will be introduced in the following.

When microgrid operates in the islanded mode, the main converter acts as a voltage source to provide a stable voltage and frequency for the ac grid. And dc grid voltage will be controlled by the battery, super-capacitor and PV boost converter.

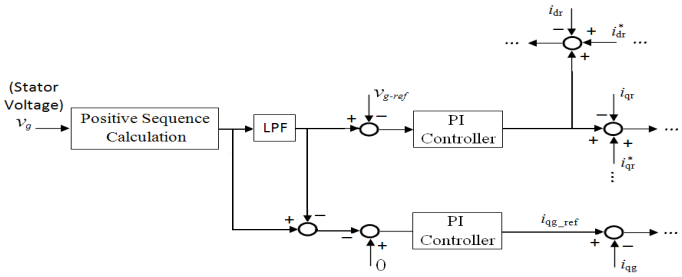

Figure7. Control schematic of the proposed voltage stabilizer applied in DFIG

1) Boost Converter Controller

In the islanded mode, PV array was considered without of MPPT controller and the new controller of the boost converter was designed as shown in Fig. 8 to support the dc bus voltage.

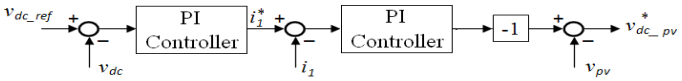

Figure 8. Block diagram of the boost converter controller in islanded mode [7]

2) Main Converter Controller

Multi-loop voltage control for a dc/ac inverter is described in [22], where the control objective is to provide a high quality ac voltage with good dynamic response at different load conditions. This control scheme was also be applied for main converter to provide high quality ac voltage in islanded mode.

3) DFIG Controller

In islanded mode, the turbine control was designed to deliver power over a range of wind conditions, taking advantage of the variable speed capability of the machine. Above about 75% rated power, the controller works in two distinct regions. When the available wind power is above the equipment rating, the blades are pitched to reduce P_{mech} delivered to the shaft down to the mechanical power 1.0 pu, thereby returning the machine equipment rating to the reference speed for full power operation, 120% of synchronous speed. When the available wind power is less than rated, the blades are fixed to maximize the mechanical power.

However, the reference speed is reduced for power levels below 0.75 pu. This behavior was included in the model by using the following equation for speed reference when the power is below 0.75 pu:

$$\omega_{ref} = -0.67P^2 + 1.42P + 0.51 \tag{2}$$

To achieve these objectives, the pitch and torque control schemes proposed in [21] were used.

IV. PSO ALGORITHM

PSO, introduced by Kennedy and Eberhart in 1995, is a swarm intelligence technique (a search method based on nature inspired systems), which is widely used in electric power systems [23]. The system initially has a population of random particles which are given some random positions and velocities in the search space. The particles have memory which is used to keep track of their previous best position, local best (P_{best}), and the corresponding fitness. The swarm has a memory which is used to keep track of the best value of all P_{best}. The search process is aimed at accelerating each particle toward its P_{best} and the swarm's global best (G_{best}). The velocity and position update equations of the particles are [24]:

$$\begin{aligned} v_i(j+1) = \omega \cdot v_i(j) + c_1 \cdot r_1 \cdot (P_{best}(j) - x(j)) \\ + c_2 \cdot r_2 \cdot (G_{best} - x(j)) \end{aligned} \tag{3}$$

$$x_i(j+1) = x_i(j) + v_i(j+1) \tag{4}$$

where ω is the inertia constant, c_1 and c_2 are two positive numbers referred as the cognitive and social acceleration constants, and r_1 and r_2 are two random numbers with uniform distribution in the interval [0, 1]. The searching procedure for the PSO technique is summarized as follows:

Step1: Initialization: A population N of particle positions and velocities are randomly initialized. In this study, N was set to be 125 and the values c_1 and c_2 were kept fixed at 2.0. Also, the weighting function was defined as follows [24]:

$$\omega = \omega_{\max} - \frac{\omega_{\max} - \omega_{\min}}{Iter_{\max}} \times Iter \tag{5}$$

where ω_{max} is final weight and ω_{min} is initial weight, selected to 0.9 and 0.4 respectively, in this study; also $Iter_{max}$ and $Iter$ are the maximum and the current iteration number, respectively. $Iter_{max}$ was set to be 35.

In the initialization, the upper and lower bounds, $X_{\max}$ and $X_{\min}$ respectively, of the parameters should be specified at first; these define the searching space. The velocity for the position updating should also be initialized randomly between $[V_{i,\min}, V_{i,\max}]$; where $V_{i,\max}$ and $V_{i,\min}$ are respectively the maximum and minimum velocities of ith particle, given by:

$$\begin{aligned} V_{i,\max} &= \frac{X_{i,\max} - X_{i,\min}}{u} \\ V_{i,\min} &= -V_{i,\max}, \qquad i = 1,2,...,150 \end{aligned} \tag{6}$$

Where $X_{i,\max}$ and $X_{i,\min}$ are the upper and lower bounds of ith particle, respectively and u is a user-defined number normally chosen between 5 and 10. In this study, position of proportional and integral gains were respectively limited in [0, 30] and [0, 600], and u was selected to 10.

Step2: Evaluation: Our objective from the PSO algorithm was to find optimal parameters in order to restore and stabilize the terminal voltage quickly. Since in the study system the islanding phenomenon was seen as the worst transient disturbance, with 100 ms as islanding detection time, so controller parameters were optimized to restore and stabilize the terminal voltage quickly, when this phenomenon was occurred. The optimization of the controllers can be done by

minimizing an error-integrating cost function. Four common types of these functions are: integrated absolute error (IAE), integrated squared error (ISE), integrated time-weighted absolute error (ITAE), and integrated time-weighted squared error (ITSE) [25]. Since ITAE yields the best performance for the considered objectives, so it was selected to be minimized as error-integrating cost function in PSO algorithm. Also, since once the islanding is occurred, ac part voltage will intensely drop, so its improvement was considered in PSO algorithm. This fitness function was mathematically defined as follows:

$$error = error_{dc} + error_{ac} + minimum\left(v_{ac\_l\text{–}l\_measured}\right) \tag{7}$$

$$error_{dc} = \sum_{t} t * \left| v_{dc\_measured}(t) - v_{dc\_ref}(=400) \right| \tag{8}$$

$$error_{ac} = \sum_{t} t * \left| v_{ac\_l\text{–}l\_measured}(t) - v_{ac\_ref}(=400) \right| \tag{9}$$

where, t is the simulation time with step-time set to $1.0*10^{-4}$ s. Also, $v_{dc\text{-}measured}$ and $v_{ac\_measured}$ are the measured dc and line-to-line ac voltages, respectively, and v_{dc_ref} and v_{ac_ref} are the reference dc and line-to-line ac voltages (i.e. both of them 400 V), respectively.

Step3: Stopping criterion: The stopping criterion was determined by $Iter_{max}$. If the iteration number is ended, then program will be stop, else go to Step 4.

Step 4: Update: The velocity updating was done by (3) while the upper and lower limits were considered as follows:

$$\begin{aligned} &if \;\; v_{i,j}(t+1) > v_{j,\max} \;\; then \;\; v_{i,j}(t+1) = v_{j,\max} \\ &if \;\; v_{i,j}(t+1) < v_{j,\min} \;\; then \;\; v_{i,j}(t+1) = v_{j,\min} \end{aligned} \tag{10}$$

Beside, the position updating was done by (4) while the upper and lower limits were handled as follows:

$$\begin{aligned} &if \;\; x_{i,j}(t+1) > x_{j,\max} \;\; then \;\; x_{i,j}(t+1) = x_{j,\max} \\ &if \;\; x_{i,j}(t+1) < x_{j,\min} \;\; then \;\; x_{i,j}(t+1) = x_{j,\min} \end{aligned} \tag{11}$$

Then, go to Step 2.

V. DYNAMIC SIMULATIONS

In this section, simulations performed in MatLab/Simulink, are shown to verify the improvement in voltage stability by the controllers with the PSO-optimized parameters compared to the original parameters. The original and optimized parameters of PI controllers are applied as shown in appendix. The voltage response of the microgrid under the islanding occurrence is shown in Figs. 9-10. The islanding detection time was considered to 100 ms. It can be seen that the response of the microgrid with the optimized-parameters based controllers is much better than that of the microgrid with original parameters.

Also, in order to investigate the robustness of the optimized parameters, simulations were performed under another large disturbance, i.e. a permanent three-phase fault occurrence (occurred between isolation transformer and main converter with 150 ms clearing time) in islanded mode. The voltage response of the microgrid under this disturbance is shown in Figs.11–12, respectively. It can be again seen that

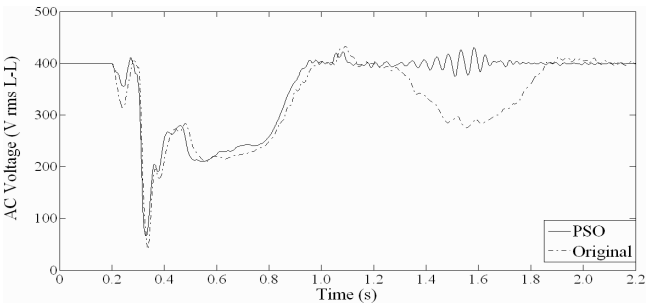

Figure 9. ac voltage waveform during the islanding occurrence

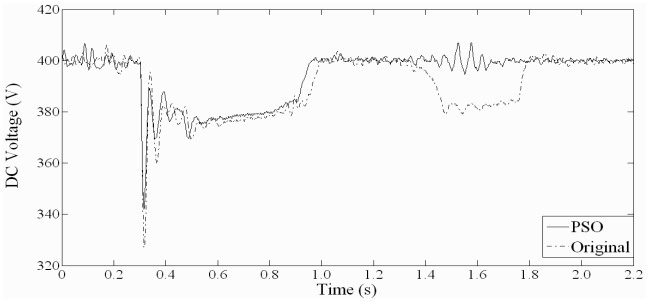

Figure 10. dc voltage waveform during the islanding occurrence

the response of the microgrid with the optimized controllers are much better than that of the microgrid with non-optimized controllers. So that with the optimized controllers, the voltage of the dc and ac grids are quickly restored and stabilized than that with the non-optimized controllers.

VI. CONCLUSION

In this paper, the controllers among the all converters were designed to improve voltage stability and dynamic voltage control in a hybrid ac/dc microgrid. Since the gains of PI controllers play an important role in stability and control of the systems, so a PSO algorithm was selected to optimize them in order to quickly restore and stabilize the voltage of both ac and dc grids. The results achieved show the efficiency of optimized controllers compared to the controllers having the original gains when the microgrid is subjected to the large disturbances.

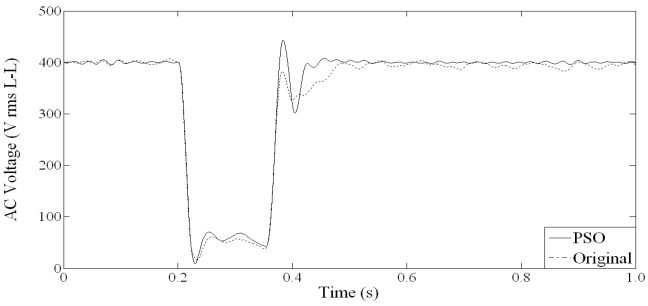

Figure 11. ac voltage waveform during the 3-phase fault occurrence

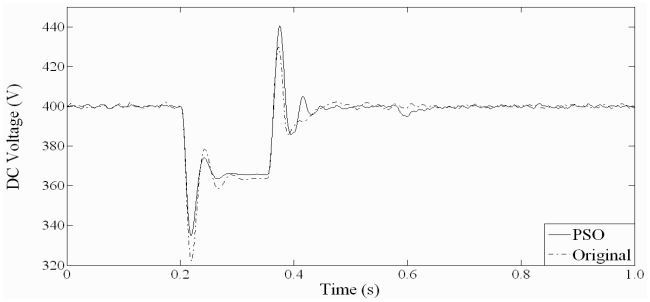

Figure 12. dc voltage waveform during the 3-phase fault occurrence

REFERENCES

[1] J. Zhenhua, and Y. Xunwei, "Hybrid DC- and AC-linked microgrids: towards integration of distributed energy resources," in IEEE Energy 2030 Conf., Atlanta, Georgia, USA, 2008, pp. 1-8.

[2] F. Katiraei, M. R. Iravani, and P. W. Lehn, "Micro-grid autonomous operation during and subsequent to islanding process," IEEE Trans. Power Del., vol. 20, no. 1, pp. 248-257, January 2005.

[3] R. Majumder, G. Ledwich, A. Ghosh, S. Chakrabarti, and F. Zare, "Droop control of converter-interfaced microsources in rural distributed generation," IEEE Trans. Power Del., vol. 25, no. 4, pp. 2768-2778, October 2010.

[4] M. B. Delghavi, and A. Yazdani, "Islanded-mode control of electronically coupled distributed-resource units under unbalanced and nonlinear load conditions," IEEE Trans. Power Del., vol. 26, no. 2, pp. 661-673, April 2011.

[5] I. J. Balaguer, Q. Lei, S. Yang, U. Supatti, and F. Z. Peng, "Control for grid-connected and intentional islanding operations of distributed power generation," IEEE Trans. Ind. Electron., vol. 58, no. 1, pp. 147-157, January 2011.

[6] H. Wang, A. M. Khambadkone, and X. Yu, "Control of parallel connected power converters for low voltage microgrid: Part II: Dynamic electrothermal modeling," IEEE Trans. Power Electron., vol. 25, no. 12, pp. 2971-2980, December 2010.

[7] X. Liu, P. Wang, and P. C. Loh, "A hybrid AC/DC microgrid and its coordination control," IEEE Trans. Smart Grid, vol .2, no. 2, pp. 278-286, Junaury 2011.

[8] D. Salomonsson, L. Söder, and A. Sannino, "An adaptive control system for a DC microgrid for data centers," IEEE Trans. Ind. Appl., vol. 44, no. 6, pp. 1910-1917, November/December, 2008.

[9] H. Kakigano, Y. Miura, and T. Ise, "Low voltage bipolar type DC microgrid for super high quality distribution," IEEE Trans. Power Electron., vol. 25, no. 12, pp. 3066-3075, December 2010.

[10] D. Salomonsson, L. Söder, and A. Sannino, "Protection of low-voltage DC microgrids," IEEE Trans. Power Del., vol. 24, no. 3, pp. 1045-1053, July 2009.

[11] T. F. Wu, K. H. Sun, C. L. Kuo, and C. H. Chang, "Predictive current controlled 5 kW single-phase bidirectional inverter with wide inductance variation for DC-microgrid applications," IEEE Trans. Power Electron., vol. 25, no. 12, pp. 3076-3084, December 2010.

[12] Z. Jiang, and X. Yu, "Power electronics interfaces for hybrid DC and AC-linked microgrids," in IEEE 6th Int. Power Electron. and Motion Control Conf. (IPEMC), Wuhan, China, 2009, pp. 730-736.

[13] D. Bo, Y. Li, and Z. Zheng, "Energy management of hybrid DC and AC bus linked microgrid," in 2nd IEEE Int. Symp. Power Electron. for Distributed Generation Syst. (PEDG), Hefei, China, 2010, pp. 713-716.

[14] C. Jin, P. C. Loh, P. Wang, Y. Mi, and F. Blaabjerg, "Autonomous operation of hybrid ac-dc microgrids," in IEEE Int. Conf. Sustainable Energy Technologies (ICSET), Sri Lanka, 2010, pp. 1-7.

[15] T.-F. Wu, K.-H. Sun, C.-L. Kuo, and C.-H. Chang, "Predictive current controlled 5 kW single-phase bi-directional inverter with wide inductance variation for dc-microgrid applications," 2011.

[16] F. S. Garcia, A. A. Ferreira, and J. A. Pomilio, "Control strategy for battery-ultracapacitor hybrid energy storage system," in 24th Annu. IEEE Appl. Power Electron. Conf. and Exposition (APEC), Washington, DC, USA, 2009, pp. 826-832.

[17] www.mathworks.com

[18] L. N. Khanh, J.-J. Seo, Y.-S. Kim, and D.-J. Won, "Power management strategies for a grid-connected PV-FC hybrid system," IEEE Trans. Power Del., vol. 25, no. 3, pp. 1874-1882, July 2010.

[19] R. Majumder, F. Shahnia, A. Ghosh, G. Ledwich, M. Wishart, and F. Zare, "Operation and control of a microgrid containing inertial and non-inertial micro sources," in IEEE Region 10 Conf. (TENCON), Singapore, 2009, pp. 1-6.

[20] R. Carriveau, Fundamental and Advanced Topics in Wind Power, J. S. Thongam, and M. Ouhrouche, MPPT Control Methods in Wind Energy Conversion Systems, InTech, 2011.

[21] N. W. Miller, J. J. S.-Gasca, W. W. Price, and R. W. Delmerico, "Dynamic modeling of GE 1.5 and 3.6 MW wind turbine generators for stability simulations," in IEEE Power Eng. Soc. General Meeting, 2003, pp. 1977-1983.

[22] N. Pogaku, M. Prodanovic, and T. C. Green, "Modeling, analysis and testing of autonomous operation of an inverter-based microgrid," IEEE Trans. Power Electron., vol. 22, no. 2, pp. 613-625, March 2007.

[23] Z. L. Gaing, "A particle swarm optimization approach for optimum design of PID controller in AVR system," IEEE Trans. Energy Convers., vol. 19, pp. 384–391, Junaury 2004.

[24] K. Y. Lee, and M. A. E.-Sharkawi, Modern Heuristic Optimization Techniques, Y. Fukuyama, Fundamentals of Particle Swarm Optimization Techniques, The Institute of Electrical and Electronics Engineers, 2008, pp. 71-87.

[25] I.-Y. Chung, W. Liu, D. A. Cartes, and K. Schoder, "Control parameter optimization for a microgrid system using particle swarm optimization," in IEEE Int. Conf. Sustainable Energy Technologies (ICSET), Singapore, 2008, pp. 837-842.

APPENDIX

Totally, there were 9 PI controllers (related to the PV array, battery storage, super-capacitor storage, and DFIG converters, and main converter) to optimize and as a result 18 controller parameters were optimized. The original and optimized parameters are given as follows:

Original PI controller parameters:

k_{p1}=13.8 pu; k_{i1}=257.8 s^{-1}; k_{p2}=13.5 pu; k_{i2}=345.8 s^{-1}; k_{p3}=17.5 pu; k_{i3}=206.8 s^{-1}; k_{p4}=20.7 pu; k_{i4}= 262.6 s^{-1}; k_{p5}=7.3 pu; k_{i5}=332.2 s^{-1}; k_{p6}=10.8 pu; k_{i6}=257.3 s^{-1}; k_{p7}=13.7 pu; k_{i7}=229 s^{-1}; k_{p8}=10.9 pu; k_{i8}=335.9 s^{-1}; k_{p9}=21.6 pu; k_{i9}=412.6 s^{-1}; k_{p10}=14.7 pu; k_{i10}=302.1 s^{-1}; k_{p11}=13.3 pu; k_{i11}=302.8 s^{-1}; k_{p12}=9.8 pu; k_{i12}=322.9 s^{-1}; k_{p13}=16 pu; k_{i13}=0 s^{-1}; k_{p14}=4.2 pu; k_{i14}=361.8 s^{-1}; k_{p15}=9 pu; k_{i15}=311.1 s^{-1}; k_{p16}=16 pu; k_{i16}=256.2 s^{-1}; k_{p17}=21.1 pu; k_{i17}= 286.1 s^{-1}; k_{p18}=13.6 pu; k_{i18}=321.6 s^{-1}

PSO-optimized PI controller parameters:

k_{p1}=2.3 pu; k_{i1}=318.5 s^{-1}; k_{p2}=28 pu; k_{i2}=341.3 s^{-1}; k_{p3}=0.4 pu; k_{i3}=97.3 s^{-1}; k_{p4}=9.3 pu; k_{i4}=99.4 s^{-1}; k_{p5}=7.9 pu; k_{i5}=413.5 s^{-1}; k_{p6}=13.5 pu; k_{i6}=1137.4 s^{-1}; k_{p7}=4.6 pu; k_{i7}=323 s^{-1}; k_{p8}=2.3 pu; k_{i8}=64 s^{-1}; k_{p9}=0.1 pu; k_{i9}=490.4 s^{-1}; k_{p10}=2.5 pu; k_{i10}=155.9 s^{-1}; k_{p11}=12.9 pu; k_{i11}=109.1 s^{-1}; k_{p12}=4.4 pu; k_{i12}=521.6 s^{-1}; k_{p13}=16.5 pu; k_{i13}=511.8 s^{-1}; k_{p14}=10.5 pu; k_{i14}=241.1 s^{-1}; k_{p15}=7.2 pu; k_{i15}=110.3 s^{-1}; k_{p16}=12.5 pu; k_{i16}=541.6 s^{-1}; k_{p17}=14.7 pu; k_{i17}=202.6 s^{-1}; k_{p18}=11.1 pu; k_{i18}=461.8 s^{-1}